CONF-
790418-- 7

On the Performance of a Field Emission Gun TEM/STEM

R. W. Carpenter and J. Bentley
REMAG, Oak Ridge National Laboratory
P. O. Box X, Oak Ridge, TN 37830

KEY WORDS: Analytical Electron Microscopy
Metallurgy
Electron Diffraction
Materials Science
Field Emission Gun
TEM/STEM Electron Microscopy

MASTER

99

Abstract

First experimental results on a Phillips EM 400 TEM/STEM fitted with a field-emission electron gun and objective "twin lens" are given here. Operation of the FEG is reliable up to maximum design voltage (120 kV). Highest resolution achieved in TEM was 1.9 Å fringe. A wide variety of diffraction modes were demonstrated, ranging from CBDP from a small area (∿10 Å dia) in STEM mode to SAD with angular resolution of 8 μrad in TEM mode. The EDS sensitivity is very high. STEM imaging performance to the highest magnifications examined (200 kx) is good. Work is in progress to evaluate the limits of STEM performance.

Introduction

This paper presents first experimental results obtained from a Philips EM 400 FEG/TEM/STEM. TEM/STEM microscopes in general are capable of a large variety of imaging, diffraction and microanalysis operational modes. These have been illustrated in detail elsewhere.[1,2] In this paper we consider basic imaging, diffraction and microanalysis performance of the instrument noted above, which differs in significant aspects from a standard EM 400. Most significant is the addition of a field emission electron gun to provide a fine, high current density probe. A special objective lens, the so-called "twin lens," is also part of the instrument. The twin lens is a wide-gap TEM/STEM lens that permits EDS with a high take-off angle and use of a high-tilt side-entry single-eucentric goniometer stage without sacrificing high-resolution performance. The twin lens is a symmetric condenser/objective of innovative design easy to use in both TEM and STEM.

This instrument will, in most instances, be applied to analysis of structural defects and local composition variations in crystalline specimens. Two applications in particular are worth noting in more detail. The first deals with the early stages of radiation damage in alloys with ordered or modulated structures. The second is the detailed analysis of interfaces such as grain boundaries and interphase interfaces; both the structural details and local chemical composition are of interest. The diffraction effects associated with local lattice parameter modulations and interfaces require high angular resolution and the highest possible signal-to-noise ratio in the recording mode. High angular resolution diffraction requires a strongly collimated incident probe, and recording of diffraction pattern fine structure requires photographic film. Thus, most structural analysis is performed in TEM or some fixed beam/film recording diffraction mode and microanalysis is done in thin areas using TEM, or STEM for maximum spatial resolution. Of central importance to both modes of operation is the performance of the field emission electron gun.

Field Emission Electron Gun Performance

The gun is of the thermally stabilized high vacuum type, and uses a single-crystal tungsten tip. The tip has a [111] direction aligned along the beam axis. The gun chamber is separated from the column by two differential pumping apertures. The gun chamber proper is evacuated by two 25 ℓ/s ion pumps and the space between the differential apertures is evacuated by a small 3 ℓ/s ion pump. Operating pressure in the gun chamber is $\sim 2 \times 10^{-10}$ torr, according to a pump current/pressure calibration curve supplied by the manufacturer.

The gun has exhibited no instabilities in operation at 100 or 120 keV. It can be operated at lower accelerating voltages, but no significant use has been made of these. The indicated emission current is usually 15 to 20 μA using an ∿3 kV extractor voltage, which is continuously variable up to 4 kV. The gun has been operated satisfactorily up to 40 μA emission current. The normal tip operating temperature is ∿1100 K. The flashing temperature used prior to start-up is usually ∿1900 K. The gun can be operated with a cold tip for short periods, if desired.

Measurements of probe current in TEM and STEM modes, using the photographic exposure measurement facilities and an exposure time/probe current calibration made with a Faraday Cup, permitted estimates of the source brightness to be made. For an accelerating voltage of 100 kV the measured probe current in TEM was $\sim 2 \times 10^{-8}$ A using a second condenser aperture of 150 μm diameter. In STEM the measured probe current was $\sim 8 \times 10^{-11}$ A using a nominal 20-μm-dia condenser aperture (probe defining aperture in STEM terminology). Brightness was calculated from[3]

$$B = \frac{4I}{\pi^2 d^2 \alpha^2} \qquad (1)$$

where I is the measured probe current, d is the probe diameter and α the illumination half-angle. The largest uncertainty in the estimate is the probe diameter, d. The manufacturer's estimated values for d are about 5 Å in STEM and 50 Å in TEM. Our measured values of α are 4 mrad in STEM and 7 mrad in TEM (see Table 1). For the I and α values measured B is estimated as 8×10^8 and 6.8×10^8 A/cm²·sr in STEM and TEM respectively. If the upper limiting probe diameters for STEM and TEM are taken to be 10 Å and 100 Å, then B is reduced to $\sim 2 \times 10^8$ A/cm²·sr in both cases, other parameters taken as constant. In a discussion of various electron sources Joy[4] compared them on the basis of B/V_0, where V_0 is the accelerating voltage. In the present case B/V_0 values between 2000 and 8000 were obtained depending on assumptions of probe diameter. These values are in or above the range given by Joy for thermally assisted and cold FEGs. Joy's estimate of tip life for a thermally assisted FEG, 100 h, has already been exceeded by a factor of 2 or 3.

In more practical terms, the exposure time for a lattice image in TEM using a silicon specimen ∿200 Å thick at an electron optical magnification of 480 kX is typically 1 s with an emission current of 15 μA. At lower magnifications, TEM pictures taken of typical metallurgical specimens (cf. Fig. 4) require somewhat longer exposures than one expects based on experience with standard TEM instruments. The usual exposure time range is 15 to 30 s. This is a result of lower total probe current in the present instrument. It has caused no experimental difficulties whatever because stage stability is high. The slight relatively high frequency flicker in illumination intensity typical of FEG sources is visible when operating in TEM mode, but has no effect on image recording. The effect does yield a noisy background in STEM images if fast scan times are used. Most of the noise can be eliminated by using longer scan times, which are also necessary to avoid clipping. No long-term drift in emission current has been observed over periods of an hour or so unless changes in tip operating temperature or extraction voltage are made during operation.

Diffraction Performance

At present all diffraction patterns are recorded on film with a static beam on the specimen. The diffraction pattern magnification can be varied over a wide range (camera length L of 4 to 680 cm) using the usual post-specimen lenses. A small-angle diffraction mode is also available. The beam tilting coils on the electron exit side of the specimen, presently used for alignment of post-specimen lenses, can be used for Grigson scanning with addition of appropriate electronics.

The diffraction capabilities of the instrument as presently used are considerably broader than conventional TEMs, due to the field emission gun/twin lens combination. First, a larger region of reciprocal space is visible than in conventional instruments, which facilitates quick orientation of specimens. Second, higher angular resolution in SAD is possible than with instruments using larger electron sources. Third, convergent beam diffraction patterns from small areas can be simply taken in either TEM or STEM mode. The limits of the viewable field in reciprocal space are shown in Fig. 1. The field is 17.3° in diameter at 120 kV. At larger camera lengths the field covers the whole final screen and is quite useful for making large tilts. It is especially useful in determining orientation differences across boundaries in polycrystalline specimens. The angular resolution available in diffraction is controlled by the second condenser lens current setting and aperture in TEM and the objective lens prefield and second condenser aperture in STEM. Table 1 lists the limiting illumination half-angles for several operating conditions. The first two modes in Table 1 produce convergent beam diffraction patterns. A wide-angle convergent beam pattern is shown in Fig. 2. The diameter of the pattern is 3.9°. Fine detail in the pattern corresponding to ∿0.1 mrad (5.7×10^{-3}°) is clearly visible. At 120 kV $2\theta_{220} = 1.0°$ for Si; in this pattern the points of the smallest sixfold star correspond to {220} Bragg positions and those of the larger sixfold star to {422} Bragg positions. A TEM convergent beam pattern taken at somewhat larger camera length is shown in Fig. 3. Higher order Laue zone lines are easily visible within the direct beam.

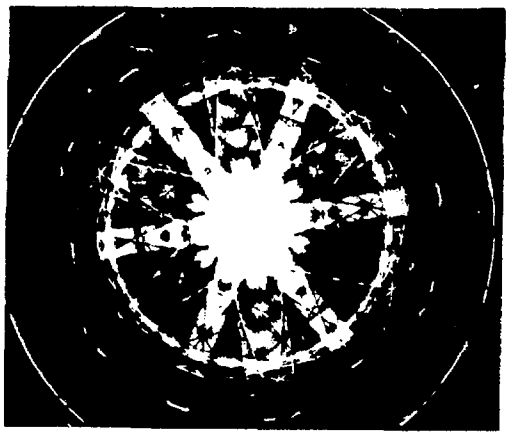

Fig. 1. Convergent beam diffraction pattern along <111> zone axis of a silicon single crystal taken at 120 kV; L = 312.4 mm. The disk of reciprocal space over which one can observe the Kikuchi pattern is 17.3° diameter. The bright ring about half-way between the zone axis and the field limit is the first-order Laue zone ring, of diameter 9.6°. Illumination half-angle α_i = 6.6 mrad; TEM mode.

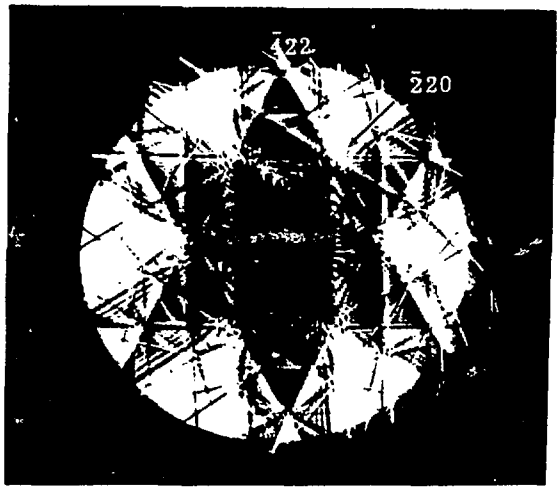

Fig. 2. Wide-angle convergent beam pattern from a silicon crystal. The beam direction is very close to <111>. Taken at 120 kV with L = 422 mm, α_i = 34.0 mrad (see text for discussion).

Table 1. Illumination Half-Angle at 120kV

	C_2 Aperture Diameter, μm		
Mode	150	100	19
STEM	34.0 mrad	22.1 mrad	4.0 mrad
TEM, convergent probe	6.6 mrad	4.4 mrad	0.8 mrad
TEM, parallel	62.9 μrad	46.2 μrad	8.2 μrad

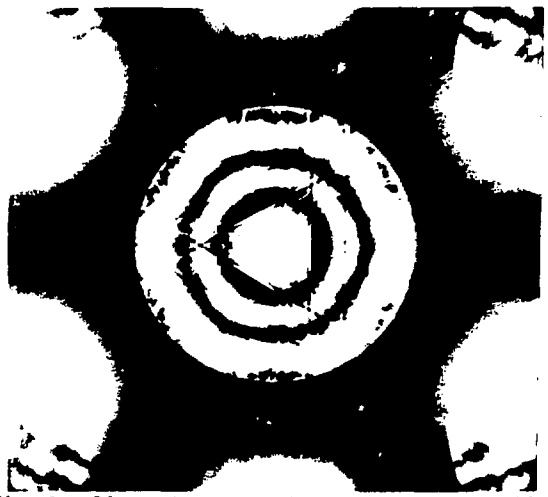

Fig. 3. Direct beam spot in convergent beam diffraction pattern from silicon at L = 153.8 cm. Taken at 120 kV along <111> α_i = 6.6 mrad. Fine structure lines are termed HOLZ lines. Note that <111> is seen immediately to be a threefold rotation axis, which is not apparent from a Bragg spot pattern of the same orientation.

Earlier research by others[5,6] showed that CBDP patterns can be used to determine a number of important specimen parameters such as lattice constant, local foil thickness and scattering factors. In the context of AEM the capability to measure local lattice parameter to an accuracy better than 1 in 1000 should form a very useful complement to microchemical analysis. This method may prove to be more sensitive to local changes in chemical composition for some materials than conventional microchemical analysis methods. The angular resolution quoted for SAD in Table 1 is higher by ~100 than that obtainable in a TEM using a conventional thermionic hairpin gun;[7] the improvement is due primarily to the use of the FEG in the present instrument.

The design of the instrument is such that the objective lens can be operated as if in STEM with the instrument in TEM mode; conversely, the second condenser lens (normally off in STEM mode) can be used in STEM to achieve continuous variation of probe size and illumination angle. Thus, the values listed in Table 1 represent limits of performance in standard STEM and TEM modes for the noted aperture sizes.

Many of the materials of interest to us are multiphase, with very small crystallites. It is expected that the diffraction capability of this instrument will provide a major advance in the structural analysis of these materials.

Imaging Performance

The microscope is typically used for structural analysis in TEM and microchemical analysis in STEM. There is no difficulty in transferring from one mode to another; typically 30 s to 1 min is required.

Examples of TEM and STEM images are shown in Fig. 4. The specimen was type 316 austenitic stainless steel. Strong <111> reflections (non-parallel) are excited in both upper and lower grains. The foil thickness is approximately 1600 Å. It can be seen that the images have essentially the same sharpness but that the contrast is somewhat reduced in STEM. This region of the specimen is thicker than one would normally choose for microchemical analysis, given a choice, but typical for many defect analysis studies. For such experiments the TEM mode is more convenient.

Another grain boundary in the same specimen is shown at higher magnification in Fig. 5. In this case the upper grain has a <111> diffraction vector strongly excited ($s \approx 0$) while no low order reflection is excited in the lower grain. It can be seen that adequate resolution is available in STEM diffraction contrast for microanalysis. These micrographs show an interesting variation on a top-bottom effect, such as discussed earlier by Fraser et al.[8] In Fig. 5(a) new fringes are added to the grain boundary fringe pattern along the top edge as the foil gets thicker; the grain boundary intersects the electron entrance surface at the bottom of the fringe pattern and the exit surface along the top of the fringe pattern. In Figs. 5(b),(c) it can be seen that contrast information is lost from the upper edge of the boundary fringe pattern, near the electron exit surface, in both TEM and STEM in this thicker region of the foil. In the experiments of Fraser et al., contrast information was lost at the exit surface in STEM, but conversely at the entrance surface in TEM. We believe the difference results from differences in diffracting conditions in the two experiments. In the present case only the top grain is in a strong diffracting condition, so the image forming beams traverse a thick region of strongly scattering material only for that part of the fringe pattern near the exit surface [i.e., along the upper part of the fringe pattern shown in Figs. 5(b),(c)]. In the work of Fraser et al.,[8] stacking faults were examined; in that case the diffracting conditions for both sides of the fault were the same, and the image forming electrons were strongly scattered through the whole foil thickness above and below the inclined fault plane. This explanation is consistent with the view that the top-bottom effect is related to inelastic scattering.

The capability of the present instrument to produce high-resolution images is of interest in view of the growing use of phase contrast images for research in materials science. A multibeam lattice image of a silicon crystal is shown in Fig. 6. The specimen was oriented with B close to [110] the foil surface normal and the area shown is about 200 Å thick. No objective aperture was used and the illumination was axial; the accelerating voltage was 100 kV. Each elliptical white dot represents a column of two-atom clusters in the [110] projection of the silicon lattice with the spacing between atoms being ∿1.36 Å. The edge-on {111} planes, spacing 3.1 Å, and {220} planes, spacing 1.9 Å, are resolved. However, it is considered possible that the 1.9 Å fringes arose from achromatic {111}-{111} interference rather than chromatic {220}-{000} interference. This resolution is not as good as that achieved by Izui and coworkers,[10] where the clusters were resolved into the two individual atoms, using a high-resolution TEM with very limited tilt capability. However, it can be considered very good for an analytical TEM/STEM equipped with a high-angle tilting stage, and is certainly adequate for lattice fringe imaging research on interfaces and order-disorder transformations in many materials of metallurgical interest. Line resolution of 2 Å (axial) has been achieved using Au crystals, where the possibility of achromatic interference does not exist. High-resolution STEM performance at this level has not yet been investigated.

Analytical Mode

The energy dispersive x-ray detector/cryostat, which is mounted on the instrument at 90° to the specimen rod eucentric tilt axis, was supplied by EDAX and is newly designed for the "twin lens" pole-piece. The detector observation direction is at 70° to the electron beam on the electron entrance side of the specimen which results in a significant improvement in P/B ratio compared to detectors at 90° to the electron beam.[11] The 30 mm^2 detector is positioned as close as possible to the specimen and subtends a large solid angle of 0.13 sr. Two spray apertures mounted in the vacuum liner tube, one on each side of the variable C_2 aperture assembly, effectively eliminate electron tails on the incident beam.[12] A non-beam defining collimating aperture is mounted in the top of the objective pole-piece. A slight to moderate high-energy x-ray fluorescence problem exists. The flux is not severe; the source is thought to be the conventional C_2 variable aperture. Installation of a thick condenser aperture is expected to reduce the problem. Relatively weak copper peaks are observed for a normal specimen holder. These can be eliminated by using a "low-background" holder.

The performance is illustrated by the analysis of an MC-type carbide precipitate shown in Fig. 7. The specimen is a carbon extraction replica from aged type 321 stainless steel.[13] The isolated precipitate, which is approximately cuboidal, of edge length ∿100 Å, constitutes $\lesssim 5 \times 10^{-18}$ g of material. The spectrum shown in Fig. 8 which contains more than enough counts for a statistically accurate analysis was obtained in the TEM mode using a 150 μm C_2 aperture with the C_2 lens at crossover. The resulting probe size was ∿100 Å. This spatial resolution is adequate for a great many applications. The fact that this is achieved solely by going to crossover with C_2 with no other changes makes this mode of analysis very straightforward and quick. Of course, for the highest spatial resolution in extremely thin specimens, where beam broadening will have its smallest detrimental effect, operation in the STEM mode will be optimum. The in-hole signal showed essentially only a copper peak and the MC precipitate is basically TiC with the constituents having atomic number Z>11 being approximately 75% Ti, 15% Cr, 6% S, 3% Ni, 1% Fe (all atomic percent).

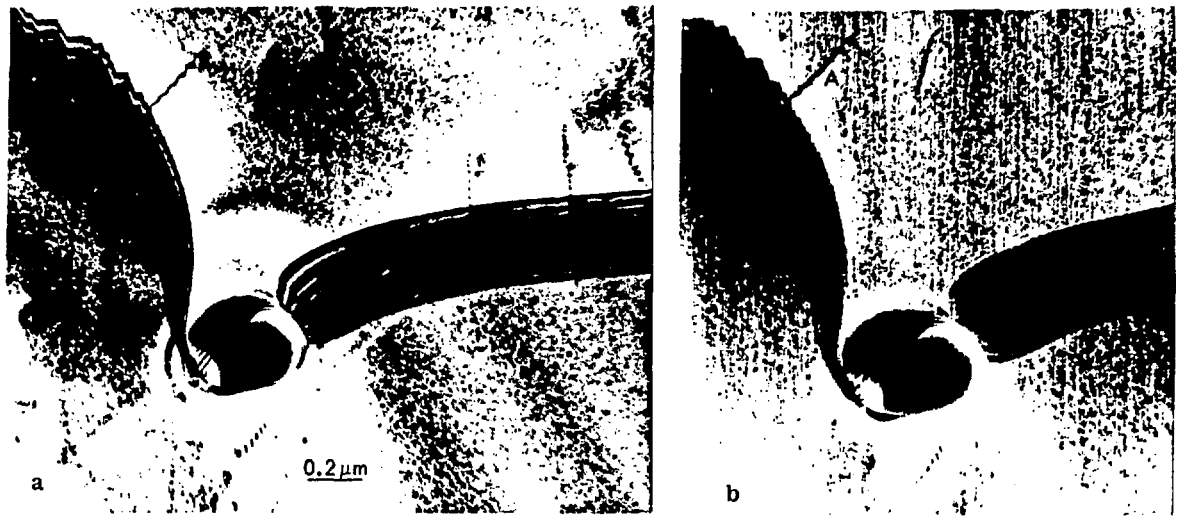

Fig. 4. TEM and STEM images of a grain boundary pinned by a non-metallic inclusion during a recrystallization annealing treatment. Strong non-parallel <111> reflections are excited in both grains. (a) TEM/BF; (b) STEM/BF. Imaging conditions: for TEM α_i = 1.0 mrad, detector half-angle = 7 mrad; STEM α_i = 4.0 mrad, detector half-angle = 7.0 mrad. Image width of dislocation A approximately 70 Å in both cases. 100 kV.

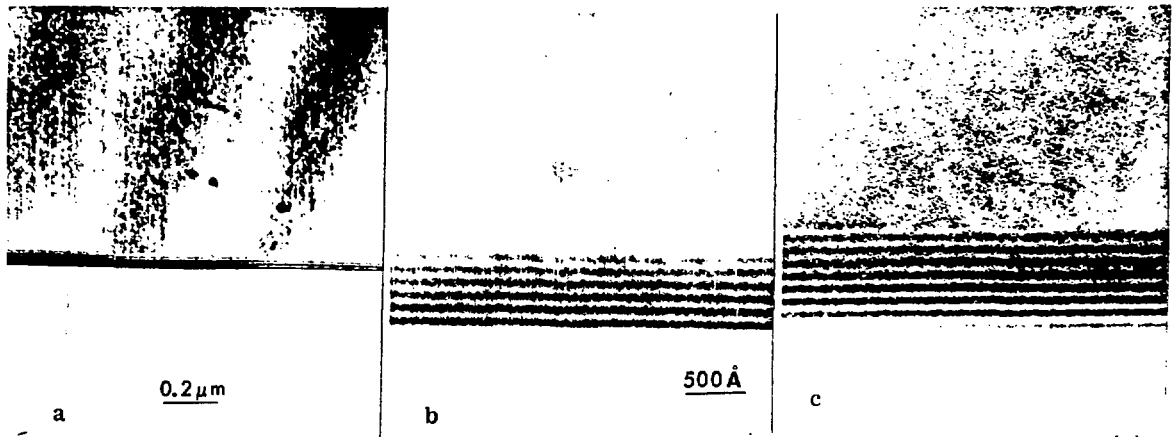

Fig. 5. A straight grain boundary in 316 ss showing the same top/bottom effect in TEM and STEM. (a) Low-magnification STEM shows additions of thickness fringes at intersection of grain boundary and bottom of foil as foil becomes thicker due to wedge; (b) high-magnification STEM shows loss of fringe image quality near bottom of foil; (c) high-magnification TEM shows loss of image quality in same area. 100 kV (see text for discussion).

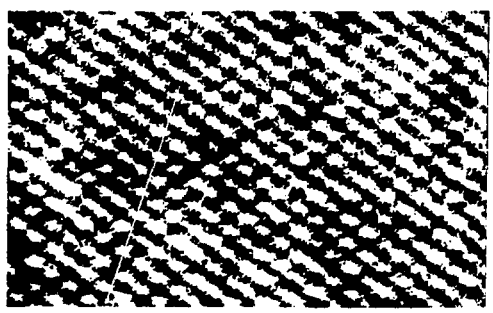

Fig. 6. A structure fringe image of a silicon single crystal taken in TEM at 100 kV with the beam aligned along [110]. Axial illumination was used at 100 kV. The {111} and {220} planes are clearly resolved.

Conclusions

All of our experience so far indicates that this instrument will operate reliably and its performance is superior to conventional TEM/STEM analytical electron microscopes. In particular the combination of high resolution in TEM, excellent diffraction performance in SAD and CBDP modes, high EDS sensitivity, and the high-tilt capability of the stage make it unique. Our results on STEM imaging so far indicate the mode produces useful images of metallurgical specimens (diffraction contrast). The principal practical difference between TEM and STEM images is somewhat reduced contrast in STEM.

Research is currently under way to evaluate the limits of STEM performance in this instrument.

Acknowledgements

This research was supported by the Division of Materials Sciences, U. S. Department of Energy, under contract No. W-7405-eng-26 with the Union Carbide Corporation. The authors acknowledge useful discussions with Drs. N. J. Zaluzec and E. A. Kenik. Finally, we would like to thank Mrs. Frances Scarboro and Mrs. Patricia White for manuscript preparation.

References

1. D. M. Maher, *Scanning Electron Diffraction in a TEM and SEM Operating in the Transmission Mode*, SEM/1974/1, IIT Research Institute, Chicago, IL, 60616, 215–224.
2. R. W. Carpenter, J. Bentley, and E. A. Kenik, *Analytical EM Investigation of Structural and Spatial Composition Variation in Lamellar Multiphase Alloys*, SEM/1977/1, IIT Research Institute, Chicago, IL, 60616, 411–424.
3. R. T. Greer, *Fundamentals of SEM for Physicists*, SEM/1976/1 IIT Research Institute, Chicago, IL, 60616, 669–674.
4. D. C. Joy, *Scanning Electron Microscopy — Where next?* SEM/1977/1, IIT Research Institute, Chicago, IL, 60616, 1–8.
5. P. M. Jones, G. M. Rackham, and J. W. Steeds, "Higher order Laue zone effects in electron diffraction and their use in lattice parameter determination," *Proc. Roy Soc. (London) A*, 354 (1977) 197–222.
6. G. Lehmpfuhl, "Convergent beam electron diffraction," pp. 305–315 in *Elec. Micros. 1978*, Vol. III, Proc. Ninth Intr. Cong. Elec. Micros., ed., J. M. Sturgess, pub by Micros. Soc. Canada, Toronto (1978).
7. R. W. Carpenter, J. Bentley, and E. A. Kenik, "Small-angle electron scattering in the TEM," *J. Appl. Cryst.* 11 (1978) 564–568.
8. H. L. Fraser, I. P. Jones, and M. H. Loretto, "Limiting factors in specimen thickness in conventional and scanning transmission EM," *Phil. Mag.* 35 (1977) 159–176.
9. P. Sieber and K. Tonar, "A Possibility of Misinterpreting Lattice Images Taken with Axial Illumination," *Optik* 44 (1976) 361–364.
10. K. Izui, S. Furuno, and H. Otsu, "Observations of cryst. structure images of Si," *J. Elec. Micros. (Japan)*, 26 (1977) 129–132.
11. N. J. Zaluzec, "Optimizing conditions for x-ray microchemical analysis in AEM," pp. 548–549 in *Elec. Micros. 1978*, Vol. 1, Proc. Ninth Intr. Cong. Elec. Micros., ed., J. M. Sturgess, pub by Micros. Soc. Canada, Toronto (1978).
12. J. Bentley et al., these proceedings.
13. J. Leitnaker and J. Bentley, "Precipitate Phases in Type 321 Stairless Steel after Aging 17 years at ∿600°C," *Met. Trans. A*, 8A (1977) 1605–1613.

Discussion with Reviewers

D. C. Joy: *Have you, or might you, consider gas processing of the tip in order to obtain greater axial brightness and superior drift and stability performance?*
Authors: We have not considered gas processing of the tip up to the present. We have not been limited by intensity or tip stability in experiments so far, but changes will be considered if necessary in the future.

S. Das: *How was the temperature of the field emission tip measured?*
Authors: The tip temperature was estimated visually. It can be seen through a window in the FEG chamber. Tip temperature could be measured directly using an optical pyrometer with optics designed for small size targets.

D. C. Joy: *Can you image the emission pattern of the cathode using the lenses of the EM400? Is the emission uniform across the cathode area or is it patchy? Is the brightest patch on axis, and does its position change with time?*
M. Hibino: *Have you measured the probe diameter for TEM? This will help you estimate the brightness more accurately.*
Authors: Yes, the tip can be imaged with the lenses. However, at the maximum magnification the emitting area is imaged as a very bright disc ∿4 mm in diameter. The emission appears to be uniform, but a magnification of over 10^6 would be necessary to determine this accurately. The brightest patch is on or very close to axis, well within the range of alignment beam tilt available. Its position changes little with time. An estimate of the TEM probe diameter at C_2 crossover can be made from the diameter of the bright spot, however the spot is not sharp-edged such as the image of the variable C_2 aperture in a convergent beam diffraction pattern, so such estimates are not very quantitative. A reasonable estimate is 60 Å. The estimate must be made visually, since the spot is so bright that a photograph taken at minimum exposure time (0.1s) is exposed to saturation in the central area.

M. Hibino: *Why do you adopt a [111] tungsten tip among the tips of any other orientations?*
Authors: Tips of several orientations were tried out for short times when the instrument was installed in August 1978. The [111] gave the best performance and has been used since, without failure.

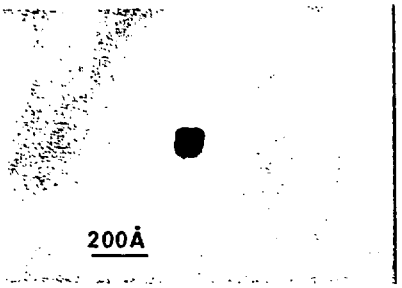

Fig. 7. TEM micrograph of a carbon extraction replica from aged type 321 stainless steel. The isolated precipitate is an MC-type carbide from which the energy-dispersive x-ray spectrum of Fig. 8 was obtained.

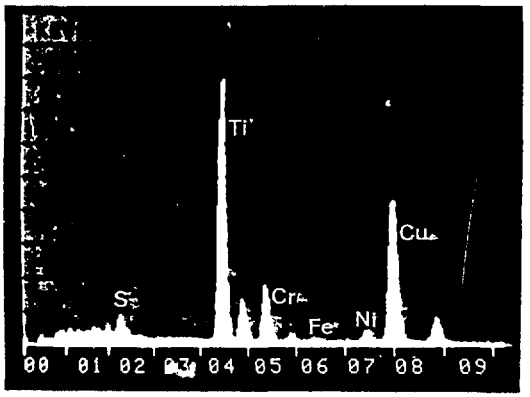

Fig. 8. Energy-dispersive x-ray spectrum of the MC-type precipitate shown in Fig. 7. Analysis time = 100 s; vertical scale = 1000 counts.

S. Das: *What is the origin of the flicker in the illumination in the field emission tip?*
Authors: No experiments have been done to determine the source of the flicker, however it may be due to continuous absorption and desorption of gas on the tip. This effect has been present on all FEG equipped microscopes the authors have operated.

D. C. Joy: *Have you attempted to estimate the lateral coherence of the beam by observing the phantom fringes beyond an edge or using Fresnel fringes? Is the value found consistent with estimate of source brightness, and have you encountered any problems (in TEM) with fringing around out-of-focus detail?*
Authors: We have not made lateral coherence estimates at large defocus. At about 0.5 μm defocus lattice fringes on a graphite foil are shifted outside the crystal image by ∿100 Å. We have not encountered serious problems in TEM with fringing around out-of-focus detail, unless the focusing error is large.

M. Hibino: *How did you measure the illumination and the detection angles? How accurate are they?*
Authors: Illumination angles were measured from the angular divergence of diffraction patterns from a crystal of known unit cell size. Detector angles were measured from the angle subtended by the detector aperture on the diffraction pattern. The values are accurate to ∿± 10%.

M. Hibino: *You mentioned three merits in the diffraction capabilities due to the FEG twin lens combination. It seems to me, however, that the essential merit is the capability of observing the brighter diffraction pattern due to the higher brightness of the gun. What did you assume as a limiting factor for the diffraction obtainable with a conventional hairpin gun? How did you get a factor of 100 as an angular resolution in SAD?*
Authors: The brightness of the diffraction is an advantage over conventional guns, particularly if one operates at long camera length and large over focus to obtain high angular resolution. There are several less obvious advantages. In many conventional microscopes convergent beam diffraction experiments are conducted with the specimen set below the objective lens, so that sufficient covergence can be achieved; this prevents reasonable imaging of the specimen area used. This restriction is avoided in the present instrument. A second advantage is the high angular resolution obtainable in the SAD mode, which is in the small-angle scattering range for thermionic gun instruments (text ref. 7). Small-angle electron scattering modes in thermionic gun instruments usually require the objective lens to be turned off, thus the area contributing to the pattern is large and not well defined (≥5.0 μm, see text ref. 2). In the present case small-angle patterns can be taken from smaller, more well defined areas. The factor of 100 increase in angular resolution results from the small electron emission area of the FEG tip, which can be demagnified to a much greater extent than a hairpin gun without reaching a loss of brightness limit (see text ref. 7).

E. L. Hall: *One major limitation in the ability to measure lattice parameters using CBED to 1 part in 1000 is contamination of the specimen. Could you comment on the presence and severity of contamination, and any precautions you have taken to minimize it?*
Authors: The reviewer is correct; on rapidly contaminating specimens HOLZ lines are eliminated within a minute. We have found that contamination rate is quite variable from one specimen to another. The rate is faster in wide-angle CBED (static beam STEM diffraction) than TEM/CBED. We have taken no special precautions to prevent contamination other than using clean specimens and passing the specimen through the airlock rapidly. Contamination of specimens does not seem a serious problem.

S. Das: *What is Grigson scanning?*
Authors: Grigson scanning is post-specimen scanning of an intensity distribution over an apertured electronic detector system. It is described in text refs. 1, 2 and R. W. Carpenter and N. J. Zaluzec, "Transmission Scanning Diffraction and Microscopy in a TEM/STEM Instrument,"

M. Hibino: *It does not seem that the imaging conditions of TEM and STEM in Fig. 4 are the same. The contrast of the STEM image may vary largely with the illumination and detection angles. Therefore it may not be possible to compare the image quality from these micrographs. Why do you think the TEM mode is more convenient?*
E. L. Hall: *The STEM image presented in Fig. 4b has markedly poorer resolution than the comparable TEM image. Are the probe size and beam current under which these images were recorded known, and could you comment on the expected ultimate spatial resolution for imaging in STEM?*
Authors: The reviewers are correct in noting that the imaging conditions for TEM and STEM are not equivalent. Note that in both cases the detector acceptance angle is larger than the illumination half-angle, and further that the illumination half-angle for STEM is larger than for TEM. The larger illumination half-angle in STEM permits a large value of Δw, where w is the dynamical deviation parameter, so that the image has less dynamical character and is dominated by anomalous transmission and has reduced contrast (see D. M. Maher and D. C. Joy "The Formation and Interpretation of Defect Images from Crystalline Materials in a STEM," *Ultra Microscopy*, *I*, (1976) 239–253). The dislocation images in the figure show this to be the case. We do not agree that the STEM images have markedly poorer resolution, based on a comparison of dislocation image width. We find TEM more convenient than STEM for most defect analysis because it is faster than STEM. Since the authors are both more experienced in TEM this bias may not be entirely correct. The probe currents used for these images were $\sim 8 \times 10^{-11}$ A (STEM) and 10^{-8} A (TEM); probe sizes were $\sim$10 Å (STEM) and 11 μm (TEM). The expected ultimate spatial resolution for STEM imaging is 2 Å line.

E. L. Hall: *What is the recording time for a STEM image?*
H. L. Fraser: *Regarding the high frequency noise in the FEG emission, the authors claim that this can be reduced in their system simply by increasing the time of exposure of a STEM image. However, the FEG/STEM images they show exhibit a rather significant contribution from this noise; why wasn't a longer exposure time used if a reduction in noise can be achieved?*
Authors: STEM images are generally recorded with 1000 lines per frame, with line times of 8, 16, 32, 64 or 125 ms. A longer exposure time was not used in this case because it was not necessary for illustration of the image characteristics of present interest.

H. L. Fraser: *On the question of the top/bottom effect associated with TEM and STEM images shown in Figs. 5, two points may be made. Firstly, the foil thickness appears to be $\sim$1500 Å (of stainless steel). It is difficult, then, to compare images in relatively thin stainless steel with those in the work of Fraser et al. (text ref. 8) where a top/bottom effect was found to be the limit of usable foil thickness. Secondly, the imaging conditions (i.e., angles) are not specified for Figs. 5; please quote these. If they are the same as those in Fig. 4, then it can be seen that in the case of TEM, a rather convergent beam was used. Calculations (ref. 8) show that fringe contrast decreases as this convergence angle increases, so that in general one might expect a decrease in fringe contrast (over the whole boundary) in the TEM image of Fig. 5c compared to the case of a parallel beam. The decrease in contrast of the fringes at the exit surface of the foil would then be explained by the use of a relatively high beam covergence in TEM, coupled with a "heavy" background level from the grain oriented for strong diffraction. A simple check on this would be to orient this grain boundary so that the grain weakly diffracting in Fig. 5c would be strongly diffracting and, conversely, the strongly diffracting grain would be weakly diffracting. Has this been done?*
Authors: The imaging conditions used in TEM were approximately the same as Fig. 4 and the STEM conditions were the same, so a rather convergent beam was used in TEM. The experiment you mentioned has been done. When the diffraction conditions are reversed, so that only the bottom grain of Fig. 5 has a low order reflection excited, the fringe contrast is poorest at the electron entrance surface, that is along the bottom edge of the fringe pattern in Fig. 5. This result holds for both TEM and STEM images. The controlling factor is the beam path length in the strongly excited grain. A long path length results in loss of image quality for both TEM and STEM.

M. Hibino: *I imagine that the images in Fig. 5 are bright field images. If so, why is the brightest area between the slightly visible broad thickness fringes in top region in Fig. 5c not brighter than the bottom region where the diffraction condition is not fulfilled? Concerning the top-bottom effect, please explain the relation between the differences in diffracting conditions for both sides of the grain boundary and the effect of the inelastic scattering in more detail. Is is not possible to explain your observation by the top-bottom effect studied by Y. Kamiya (J. Electron Microscopy, 22 231 (1973)?*
Authors: The images are BF. In the top grain $s \approx 0$, so that strong diffraction occurs everywhere. In the bottom diffraction is weak and little diffracted intensity is blocked by the objective aperture. Thus the bottom grain appears brighter. The diffracting conditions were arranged so that a low order $\bar{g}$ (<111> in this case) was excited in the upper grain, and no low order $\bar{g}$ was strongly excited in the lower grain. Inelastic scattering degrades that part of the grain boundary fringe image where strongly diffracted beams have the longest path length through an excited crystal (see answer to H. L. Fraser's question above). It does not seem possible to explain the present results using Kamiya's top/bottom study, since the

diffracting conditions change drastically across the boundary in the present case.

H. L. Fraser: *It is stated that a "moderate" x-ray fluorescence problem exists. What is meant by "moderate," e.g., what percentage of the Ni-peak in the spectrum of Fig. 8 is produced by x-ray fluorescence? How have spectral contributions from stray electron radiation been reduced?*
Authors: As stated in the text the only detectable peaks in the "in-hole" spectrum were Cu K lines. However, an extraction replica is a poor test specimen with which to evaluate the extent of uncollimated fluorescing radiation (text reference 12). Using a self-supporting thinned disk of β-NiAl the Ni K_α intensity of the in-hole signal amounted to ∿7% of the Ni K_α signal from an area of the foil of ∿60 nm thickness. As mentioned in the text, spray apertures (installed by the manufacturer) on each side of the variable C_2 aperture assembly effectively eliminate "electron tails."

H. L. Fraser: *You mention that the Cu-systems peak is either weak or absent depending on which specimen holder is used. However, it seems that in Fig. 8, there is a significant Cu K_α peak present at ∿8. keV. How are your statements and results rationalized?*
Authors: The Cu K lines in Fig. 8 originate from both the specimen holder and the support grid for the extraction replica. The intensity is approximately twice the in-hole Cu signal (which is due to fluorescence by uncollimated high energy x-rays produced in the condenser system). The remaining 50% of the Cu signal is due to fluorescence by specimen generated radiation (for details, see text reference 12). Self-supporting specimens or extractions on Be grids result in much smaller Cu systems peaks.

M. Hibino: *Could you please give the electron probe current you used for x-ray analysis of the MC-type precipitate? Did you notice any effect of contamination and specimen/electron probe drift during the analysis time? What is your estimation for possible higher spatial resolution of x-ray analysis in your instrument?*
Authors: A probe current of 8nA was used and no visible contamination was visible after the 100s analysis time (Fig. 7 was taken after the analysis). The TEM image was viewed continuously during the analysis and the amount of specimen/electron probe drift was estimated to be <2 nm.

It is not yet clear what will be the limiting factor for the spatial resolution of x-ray analysis. Available current in small probes will probably not be the limiting factor because of the large detector collection angle. Drift or beam spreading within the specimen are more likely candidates. Certainly, a resolution <5 nm appears possible.

S. Das: *Would the authors comment on how the performance of their instrument compares with the performance of other dedicated STEM (e.g., VG microscopes)?*

Authors: Direct comparisons between TEM/STEMs and D-STEMs are difficult because two different design concepts are used. From a materials science viewpoint the additional diffraction capabilities available in a TEM/STEM (if fitted with an FEG) in the form of high angular resolution and very high S/N for film recorded patterns are quite useful. The TEM/SAD image/diffraction capability is often faster for setting up a specific diffraction condition and recording the image than the equivalent operations in a D-STEM. On the other hand, if one is interested in direct quantitative recording of intensity distributions from diffraction patterns or images a TEM/STEM must usually be fitted with special (Grigson) scanning coils; D-STEMs can normally operate in this mode. It is fair to say that scanning signal processing electronics are more advanced in D-STEMs than TEM/STEMs in present commercial instruments. The analytical capabilities (EDS, EELS) of the two types depend as much on spectrometer design and interfacing as on the instruments themselves, and are still in development, especially EELS.